Numerical study on wind pressures caused by the variation of the rounding radii of the industrial shed eaves

GUILHERME S. TEIXEIRA, MARCO D. DE CAMPOS
Institute of Exact and Earth Sciences
Federal University of Mato Grosso,
Av. Valdon Varjão, 6390, Barra do Garças, 78605-091, Mato Grosso, BRAZIL

Abstract: This work approached a typical industrial shed with varied rounded eaves, which is pointed out, in the few papers on it, as favorable to structural safety against the action of the winds. Since the literature has neglected this building configuration, the external pressure coefficients were obtained by CFD with the aid of the *Ansys Workbench* software, applying tetrahedral meshes in the domain discretization. Furthermore, the boundary layer around the building was modeled for greater accuracy in data capture. Using the *RNG K-Epsilon* model, were determined the turbulent flow effects. The results indicated a reduction in the pressure coefficients in the most sensitive regions and prone to accidents caused by wind on the roof. Finally, the flow pattern can be measured using the presented velocity fields.

Key-Words: Wind action, industrial shed, eaves, *Ansys,* pressure coefficient.

Received: April 9, 2022. Revised: March 5, 2023. Accepted: April 3, 2023. Published: April 25, 2023.

1 Introduction

In the last 50 years, it has taken advantage of electronic instrumentation development and computer-based statistical analysis techniques for conducting various surveys of wind loads on low-rise buildings. Despite this, there were few studies about the wind loads in the curved eaves in industrial and commercial low-rise buildings [1].

This approach is necessary since curved eaves may mitigate the high suctions that develop with conventional sharp eaves over the lower part of the windward roof slope. It is precisely this suction that usually causes damage to the structure [2].

In this context, a low-rise buildings experiment of 1986/87, the *Silsoe Structures Building*, in the United Kingdom, was idealized for full-scale wind pressure measurements. This building, constructed in an open country, constituted an optional eaves geometry with either traditional sharp or curved eaves. As well as seventy pressure tapping points on the building roof and walls, the building was equipped with twelve strain gauge positions on the central portal frame to enable measurements of structural response to be made ([1], [3]).

Despite the studies already carried out on geometric factors of buildings such as roof slope, height-depth ratio, and width-depth ratio, few studies have focused on analyzing the influence of eaves. Among these, few presented results for rounded eaves. Few authors in literature, such as the *Silsoe Structure experiments* ([4],[5],[6]), addressed this architectural element. Thus, this work analyzed the influence on the pressure coefficients caused by the variation of the rounding radii of the eaves.

2 Methodology

ANSYS Workbench (often ANSYS WB) is a multi-disciplinary business software widely used in industry and academia applications. It is known by researchers in the computational field, especially in Wind Engineering, its integrity, and cost-effectiveness in the study of wind action on buildings. For these reasons, the present work was almost entirely developed using the software, from geometry modeling, meshes, equations solution, and post-processing, and described next.

Geometry, domain, and subdomain

The basic geometry of this work consists of a shed located in the farmland of the *Silsoe Research Institute*. It is a building with a rectangular plan measuring 12.90x24.10x4.16 m (WxLxH), eaves rounding radius of 635 mm (varying in the simulations), and roof pitch of 10º [2], modeled using *SpaceClaim*, *Ansys WB CAD platform* (Fig. 1a). For the domain, were adopted the recommendations of [7], being the length of 5H+L+15H, the width of 5H+B+5H, and the height of H+5H, dependent on the building height of (H=4.16 m), of the length L of the building in the flow direction and width B. Note that the reference height H=4.16 m is measured from the ground to the

projection of the sharp eaves, as in the studies conducted in [8], instead of the height up to the ridge. For better accuracy of the effects of the flow in the vicinity of the building, a subdomain with dimensions of 0.5H in all directions of the building was developed (Fig. 1b). The blockage ratio varied from 4.47% to 5.14% in the simulations, above the 3% recommended by [7] but below the maximum of 10% indicated, which may be enough to avoid artificial acceleration of the flow over the building.

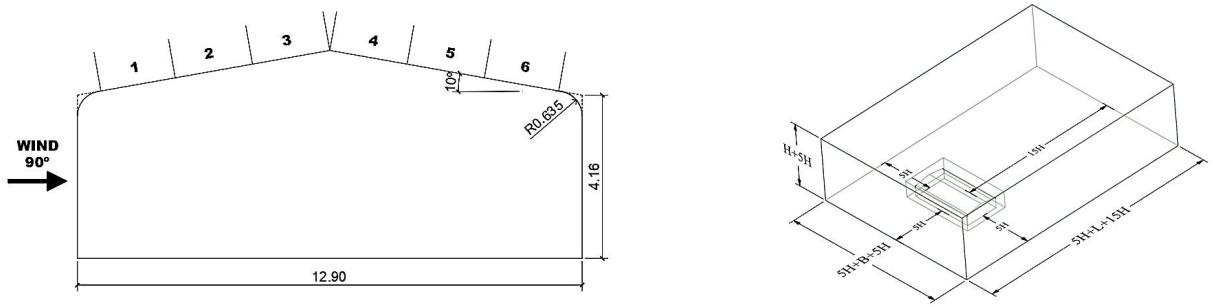

(a) (b)

Fig. 1 (a) Geometry cross-section, with roof, equally divided into six zones, and (b) domain, subdomain, and building (both in meters).

Mesh

Mesh represents a fundamental step in attaining the numerical solutions to the governing partial differential equations using CFD because the mesh selected for CFD simulations will define the accuracy and resolution of the simulation results, both of which will affect the computation time and level of detail in the results [9]. Likewise, in this work, some precautions were adopted, which used unstructured meshes composed of tetrahedral, allowing better parameterization and control in critical regions [10].

It's them:

i) The capture of proximity and curvature: these parameters are relevant to capture the effects in the rounded regions of the eaves.

ii) In the meshes were considered four refinement levels (Fig. 2). The first is in the fluid domain, with a controlled dimension of the elements; the second is in the subdomain, with a lesser in size element than the previous one (half); in the third level, the control of the size of the elements on the faces of the building and, finally, the modeling of the boundary layer.

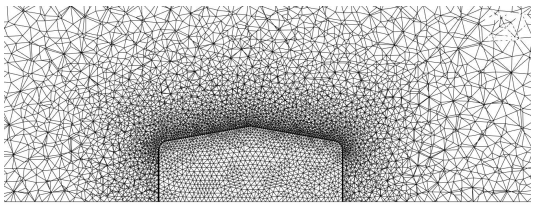

Fig. 2 Mesh refinement levels used of one numerical application in this work

For the external flows, i.e., bodies immersed in fluid streams with unconfined flows, viscous effects will be present at the solid-fluid boundaries [11]. Global effects on the flow can happen due to the tensions existing in these thin boundaries (called *boundary layers*, described in [12]). For this reason, its CFD modeling is relevant and used in the present work. To determine the boundary layer parameters were adopted the recommendations of the *ANSYS CFX-Solver Modeling Guide* [13]:

$$\delta = 0.035\ L\ Re$$

δ is the boundary layer thickness, L = D_h the hydraulic diameter, and *Re* the Reynolds number, given by:

$$D_h = \frac{4A}{2a + 2b}$$

$$Re = \frac{V\ D_h}{\upsilon}$$

being *A* the cross-sectional area of the wind tunnel to the airflow, *a, b* the horizontal and vertical dimension of the cross-section of the control volume to the airflow, respectively, *V* the flow velocity [m/s] and υ the air kinematic viscosity (=1,56E-5 [m²/s]).

In addition, 10 nodal points in the direction orthogonal to the flow obstruction wall, according to [13]. This number of points was adopted to guarantee a good performance of the turbulence model. It was also considered the boundary layer on the 4 facades, on the roofs, and on the eaves of the shed. Although the expansion rate applied to the meshes is 1.1 (below the maximum 1.2 usually recommended by ANSYS), in the boundary layer, exclusively, the expansion rate of the elements was [14]:

$$Growth\ rate = \left(\frac{\delta}{\Delta y}\right)^{1/14}$$

where Δy represents the thickness of the first element and is given by [13]:

$$\Delta y = \sqrt{74}\, D_h Re^{-13/14}$$

iii) In this work a grid sensitivity analysis was to ensure that the results, depending on the mesh employed, did not present significant changes. Thus, three different grids were applied for each simulation (coarse, medium and fine), having

approximately 660k, 1.13Mi, and 2.30Mi grid cells, respectively. This addition of cells at each new mesh iteration was always greater than 1.5 times the previous mesh, as indicated by [16]. Even with the meshes not showing significant differences in the results, the fine meshes.

iv) Mesh quality parameters are also fundamental factors to guarantee an acceptable mesh. Here, the aspect ratio, skewness, and orthogonal quality were analyzed, as they describe well the geometric aspects and connectivity between elements. For three-dimensional elements, the aspect ratio is the ratio between the radius of the circumscribed and inscribed circles in the base geometry (in our case, the triangles). The skewness indicates how close to the ideal geometry (in this case, tetrahedron) the mesh cells or faces are (recommended values between 0 and 0.5). Lastly, the orthogonal quality metrics the element's orthogonality (recommended values close to 1) [15].

v) Finally, concomitantly with the grid sensitivity analysis, studies were carried out with meshes of different methodologies to certify the independence of the results.

Thus, in the analysis, it was restricted to meshes with one level of refinement. In these, only the size of the element in the fluid domain would be under the user's control.

Although, for these two methodologies, the differences in the results were not significant, the first methodology resulted in values closer to those of the literature adopted in the validation and, therefore, was adopted in this work.

Setup and solver setting

The vertical profile of wind speeds on the INLET face is described below by the Power Law, which is widely accepted in Engineering applications [17]:

$$\frac{U_z}{U_{ref}} = \left(\frac{Z}{Z_{ref}}\right)^{\alpha}$$

where U_z is the wind speed (in meters per second) at height Z (in meters), and U_{ref} is the pre-established wind speed at a reference height Z_{ref}, adopted as 10 m. The exponent α is an empirically derived coefficient that varies depending on the terrain roughness and the time interval. Also, α=0.16 representing a terrain with high grass, and U_{ref} =30m/s were adopted.

At different points and times within the fluid domain, a turbulence model frequently used in Wind Engineering, the *RNG K-Epsilon*, was employed to model the random properties of the turbulent flow [18].

According to Franke *et al.* [19], the advective terms must be discretized using higher-order schemes when transforming the governing differential equations into algebraic equations. For this, in the present work, the *High Resolution schemes* for such terms and numerical turbulence were defined. As the simulations involve a notably free surface [13], was applied the Double Precision scheme (16 digits) to improve the convergence.

In addition, the chosen stopping criterion was the RMS equal to 10E-4, followed by three verification steps to determine the reliability of the results:

i) Interpretation of the results of the residual values of the mass, momentum, energy, and additional turbulence equations due to the *RNG K-Epsilon model* employed. That is, residual RMS, in addition to the simulation stopping criterion, was used as a convergence criterion.

ii) Monitoring the *Principle of Conservation of Mass.*

According to [13], the difference in mass on the INLET and OUTLET faces must be less than 1%.

iii) On the physical coherence of the results.

The external pressure coefficients, defined by $Cpe=\Delta p/q$, where *Cpe* is the external pressure coefficient; Δp is the difference in external pressure coefficient, and q is the dynamic pressure, in addition to being used to analyze each application, provide parameters for interpreting the correct physics of the values obtained with the simulation. This fact is due to the range of expected values for this parameter. For positive values, which indicate overpressures, a maximum of *Cpe*=1.0 is expected (disregarding errors associated with CFD). For negative values, which indicate suction, in defined regions of geometry, the magnitude can be from 6 to 8 times the pressure obstruction [20]. Finally, Table 1 shows the rest boundary conditions adopted.

Table 1. Boundary conditions and parameters.

Condition	Parameters
Method of mesh	Tetrahedron
Capture curvature and proximity	On
Reference pressure	101325 [Pa]
Air temperature	25º [C]
Turbulence intensity	Medium (5%)
Flow regime	Subsonic
Inlet	$U/U_{ref} = (Z/Z_{ref})^{\alpha}$
α	0.16
Z_{ref}	10 [m]
U_{ref}	30 [m/s]
Relative pressure of outlet	0 [Pa]
Wall - Ground	Rough wall
Model wall roughness	Smooth wall
Roughness	0.01 [m]
Advection scheme	High resolution
Turbulence numeric	High resolution
Minimum number of iterations	100
Maximum number of iterations	500

3 Numerical results

Application 1 (*validation*): To validate the methodology, the *T-test* was used to evaluate the

significant differences between the means of the samples of the present work and of [2]. In [2], the results used the full-scale field experiment, which has a significant quality in terms of benchmark if compared with the reduced models, which minimized the scale effects ([21], [22]). The angle of incidence was 90º with wind reaching the building transversally (named *Model 1*, where the notation "*R plus three digits*" represents the rounding for the eaves, in mm), and Tables 2 and 3 show the mesh parameters.

The sensitivity of roof pressures as a function of eaves configurations is well described in the literature ([23], [24], [25]). Thus, to adequately represent the results, the samples for the test were composed of the average external pressure coefficients of the windward and leeward roofs (not including the eaves themselves) (Fig 3a). A transverse cut sectioned the surface into six equal parts (Fig 1a). Table 4 shows the *Cpe* values for six zones using *Model 1* in comparison with [2].

Considering the *null hypothesis* (H_0) that the means are not different, assuming two samples with equivalent variances, two-tailed distribution, and significance $\alpha' = 0.05$, using *Microsoft Excel software* obtained a *p-value* = 0.836, approximately. As *p-value* > α', we do not reject the null hypothesis (H_0) and, therefore, consider the difference between the means in the *Cpe* values insignificant.

Table 2. Mesh quality parameters.

			Results		
Parameter	**Range**	**Classification [12]**	**Model 1 (R635) (average)**	**Model 2 (R335) (average)**	**Model 3 (R935) (average)**
Aspect ratio	up to 100	recomended	51.364	59.786	54.655
Skewness	0.25-0.50	good	0.25065	0.2566	0.25389
Orthogonal quality	0.70-0.95	good	0.74538	0.73935	0.74254

Table 3. Results for the boundary layer of *Models 1*, *2* and *3* with vent at 90º.

***V* (m/s)**	**a (m)**	**b (m)**	***A* (m²)**	***D_h* (m)**	***Re***	**δ (m)**	**Δ*y* (m)**	***Growth rate***
30	65.7	24.96	1639.87	36.18	69569821	9,59724175E-2	1,62477E-5	1.859

Table 4. *Cpe* values for six zones using *Model 1* in comparison with [2].

	***Cpe* medium**					
Model	**Zones**					
	1	2	3	4	5	6
[2]	-0.80	-0.55	-0.79	-0.80	-0.39	-0.25
Present work	-0.91	-0.49	-0.94	-0.96	-0.32	-0.17

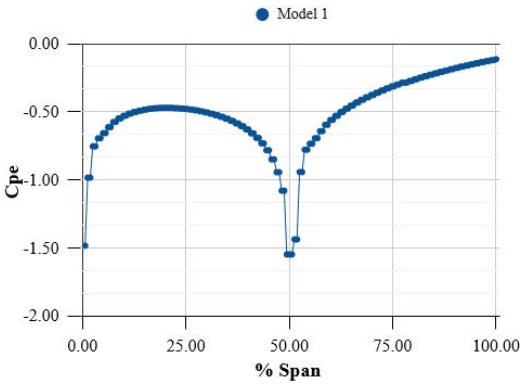

(a)

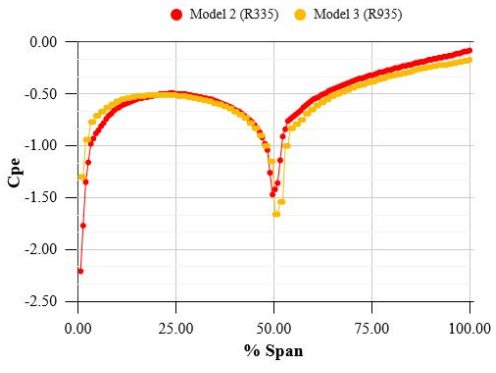

(b)

Fig. 3 Pressure distributions over roof for curved eaves with transverse wind for (a) *Model 1,* and (b) *Models 2* and *3.*

Application 2 (*eaves rounding radii*): Here, the rounding radii of the eaves were varied to analyze their influence on the pressure coefficients. According to the results, the roofs presented a similar distribution pattern, with suction peaks on the windward eaves and ridges. Despite this, the intensity at the point immediately beyond the windward eaves (i.e., close to 0.00% of the roof span) in Model 2 was 41.18% higher than in Model 3, although it was 22.06% lower in the ridge (Fig 3b). Analogously to the results of [2], the smaller the rounding radius (in this work, R335 < R935, and

in [2], R000 (sharp eaves) < R635), the more intense were the pressure coefficients at the most windward point of the roof (~0.00 % span). As in [2], an inversion of intensities in the ridge. The values were close on the leeward face of the roof, with an absolute difference for *Cpe* of 0.10.The results also showed that in the eaves themselves, the smaller the radius, the greater the suctions (Fig. 4a-b).

In consonance with this result, a sharper curve with smaller radii will cause an increase in the flow velocity (Fig. 4c-d). Hence, based on the literature, [26], [27, [28], or on Bernoulli's Theorem, it is concluded that the most intense velocities generated the highest negative pressure peaks. Also, the point of displacement occurred approximately in the middle of the leeward roof, compared to the building with the eaves with a larger radius (*Model 3*), in line with [2] (Fig. 4c-d).

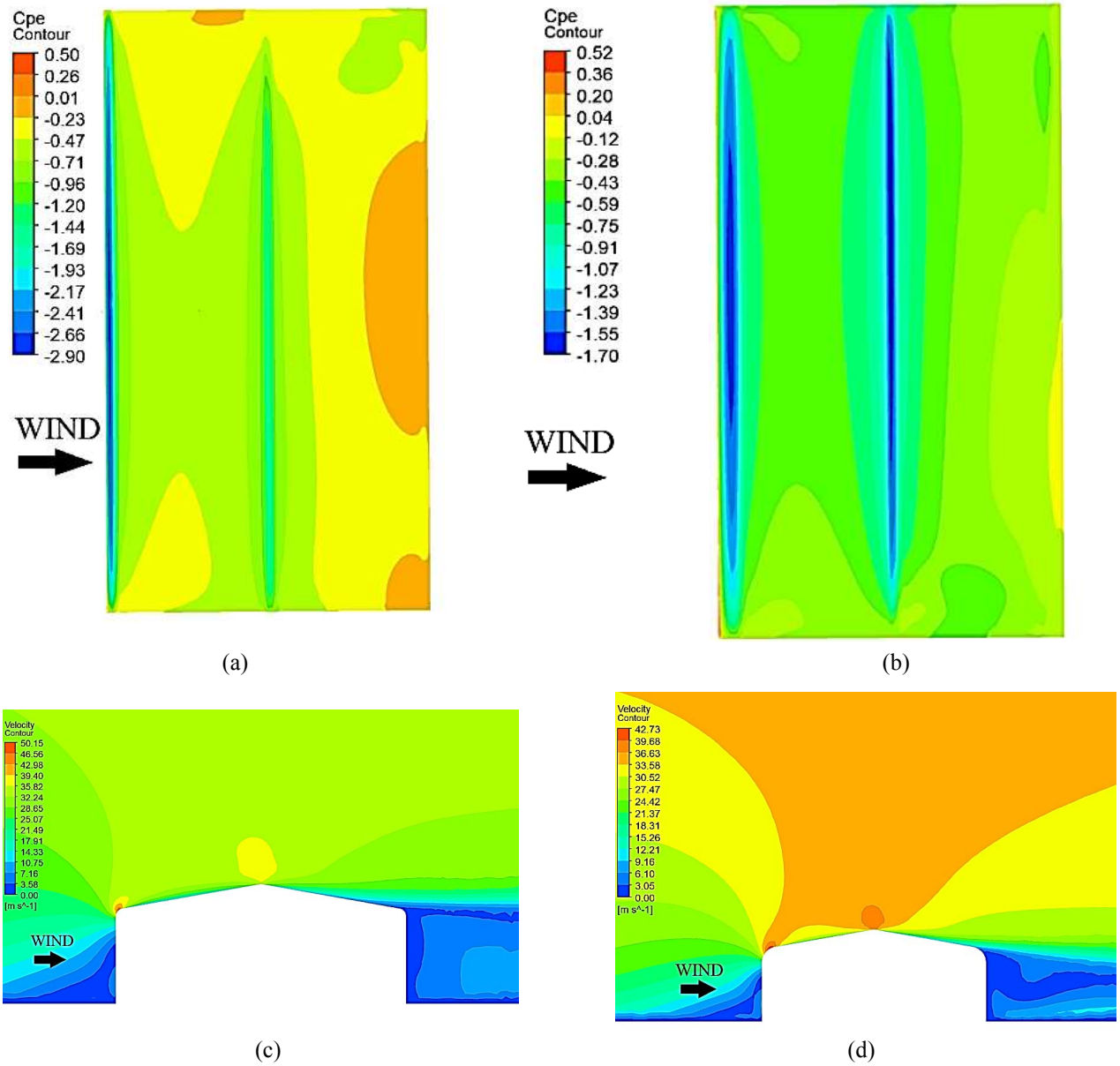

Fig 4 Top view *Cpe* contour and the transverse plane of the velocity fields, respectively, for (a), (c) *Model 2*, and (b), (d) *Model 3*.

4 Conclusions

The effects of wind on the roofs of buildings with curved eaves were measured using computer simulation.

The results for two rounding radii presented here corroborate the literature, i.e., increasing the radius of the eaves can decrease the pressures on the roof portions closer to the windward side, despite generating great efforts on the ridge.

Furthermore, the configurations of the rounded edges can be considered of little relevance when the leeward faces are analyzed.

These results help to create more references for Wind Engineering, considering that the literature addressing rounded eaves is scarce. Future research

should test new radii and seek to establish connections with roof slopes, height-depth ratio, and width-depth ratio, among other relevant geometric aspects.

References:

[1] J. D. Holmes, *Wind Loading of Structures*. London: Spon Press, 2001.

[2] A. P. Robertson, Effect of eaves detail on wind pressures over an industrial building, *Journal of Wind Engineering and Industrial Aerodynamics*, Vol. 38, 1991, pp. 325-333.

[3] G. M. Richardson, R. P. Hoxey, A. P. Robertson and J. L. Short, The Silsoe Structures Building: comparisons of pressures measured at full scale and in two wind tunnels, *Journal of Wind Engineering and Industrial Aerodynamics*, Vol. 72, 1997, pp. 187-197.

[4] R. P. Hoxey and P. J. Richards, Flow patterns and pressure field around a full-scale building, *Journal of Wind Engineering and Industrial Aerodynamics*, Vol. 50, 1993, pp. 203-212.

[5] G. M. Richardson, A. P. Robertson, R. P. Hoxey and D. Surry. Full-scale and Model Investigations of Pressures on an Industrial/Agricultural Building. *Journal of Wind Engineering and Industrial Aerodynamics*, Vol. 36, 1990, pp. 1053-1062.

[6] Savory, S. Dalley and N. Toy. The effects of eaves geometry, model scale and approach flow conditions on portal frame building wind loads. *Journal of Wind Engineering and Industrial Aerodynamics*, Vol. 41-44, 1992, pp. 1665-1676.

[7] J. Franke, A. Hellsten, H. Schlünzen and B. Carissimo, *Best practice guide for the CFD simulation of flows in the urban environment, COST Action 732: Quality assurance and improvement of microscale meteorological models.* Hamburg: COST Office, 2007.

[8] N. S. Fouad, G. H. Mahmoud and N. E. Nasr, Comparative study of international codes wind loads and CFD results for low rise buildings, *Alexandria Engineering Journal,* Vol. 57, 2018, pp. 3623–3639.

[9] J. Tu, G. H. Yeoh and C. Liu, *Computational Fluid Dynamics: a practical approach*. 3rd edition, Butterworth-Heinemann, 2018.

[10] M. D. Galter, I. Vizotto, A. M. Ferreira and S. Cardenas. Ação do vento em modelo de casca de forma livre de planta pentagonal apoiada nos vértices. In: *XXXVI Iberian Latin American Congress on Computational Methods in Engineering*, Rio de Janeiro, 2015 (*in Portuguese*).

[11] F. White and H. Xue, *Fluid Mechanics*, 9th Ed. McGraw Hill, 2021.

[12] J. A. D. Ackroyd, B. P. Axcell and A. Ruban, *Early developments of modern Aerodynamics,* Elsevier, 2001

[13] ANSYS, *CFX-Solver Modeling Guide Ansys*, Canonsburg, 2021.

[14] M. S. C. Garcia, I. Vizotto, A. M. Ferreira and S. Cardenas. Hexagonal free form shell supported on six vertices under the wind pressures. In: *XXXVI Iberian Latin American Congress on Computational Methods in Engineering*, Rio de Janeiro, 2015.

[15] ANSYS, *ANSYS Meshing User's Guide*, Canonsburg, 2021.

[16] Y. Tominaga, A. Mochida, R. Yoshie, H. Kataoke, T. Nozu, M. Yoshikawa and T.Shirasawa, AIJ guidelines for practical applications of CFD to pedestrian wind environment around buildings, *Journal of Wind Engineering and Industrial Aerodynamics*, Vol. 96, No. 10-11, 2008, pp. 1749-1761.

[17] J. Blessmann, *O vento na Engenharia Estrutural*, 2nd Ed., Porto Alegre: UFRGS, 2013 (*in Portuguese*).

[18] J. Revuz, D. M. Hargreaves and J.S. Owen, On the domain size for the steady-state CFD modelling of a tall building, *Wind and Structures*, Vol. 15, No. 4, 2012, pp. 313-329.

[19] J. Franke, C. Hirsch, A. G. Jensen, H. W. Krüs, M. Schatzmann, P. S. Westbury, S. D. Miles, J. A. Wisse and N. G. Wright, *Recommendations on the use of CFD in predicting pedestrian wind environment , COST Action C14: Impact of Wind and Storms on City Life and Built Environment. Hamburg*, COST Office, 2004.

[20] S. T. Manfrim, R. Bertolino Jr., Estudo numérico da determinação das pressões devido a ação do vento em edifícios industriais. In: *XXXII Jornadas Sulamericanas de Engenharia Estrutural*, 2006, pp. 2059-2068 (*in Portuguese*).

[21] S. K. Chakrabarti, Physical Modelling of Offshore Structures, *In*: S. K. Chakrabarti (Ed.), *Handbook of Offshore Engineering,* Elsevier, 2005, Chap. 13, pp. 1001-1054.

[22] H. J. Leutheusser, Influence of architectural features on the static wind loading of buildings, In: *Proceedings of Technical Meeting Concerning Wind Loads on Buildings and Structures: Held at National Bureau of Standards*, 1969, Gaithersburg, Building Science Series 30, 1969, pp. 73-86.

[23] P. Huang, X. Peng and M. Gu, Aerodynamic devices to mitigate rooftop suctions on a gable roof building. *Journal of Wind Engineering and Industrial Aerodynamics*, Vol. 135, 20141, pp. 90-104.

[24] R. P. Hoxey and P. Moran, A full-scale study of the geometric parameters that influence wind loads on low rise buildings, *Journal of Wind Engineering and Industrial Aerodynamics*, Vol. 13, 1983, pp. 277-288.

[25] P. Huang, L. Tao, M. Gu and Y. Quan, Experimental study of wind loads on gable roofs of low-rise buildings with overhangs, *Frontiers of Structural and Civil Engineering*, Vol. 12, 2016, pp. 300-317.

[26] D. D. Flynn, H. Hemida, D. Soper, C. Baker. Detached-eddy simulation of the slipstream of an operational freight train. *Journal of Wind Engineering and Industrial Aerodynamics*, Vol. 132, 2014, pp. 1-12.

[27] A. C. Khanduri, T. Stathopoulos and C. Bédard. Wind-induced interference effects on buildings - a review of the state-of-the-art. *Engineering Structures*, Vol 20, No. 7, 1998, pp. 617-630.

[28] P. P. Mendis, T. Ngo, N. Haritos, A. Hira, B. Samali, J. Cheung. Wind Loading on Tall Buildings. *EJSE Special Issue: Loading on Structures*, 2007, pp. 41-54.

Contribution of individual authors to the creation of a scientific article

Guilherme Teixeira was responsible for the methodology, carrying out the simulation, and writing the results. Marco Campos carried out the conceptualization, review, and editing.

Sources of Funding for Research Presented in a Scientific Article or Scientific Article Itself

No funding was received for conducting this study.

Conflicts of Interest

The authors have no conflicts of interest to declare that are relevant to the content of this article.